Click Here for Full Article

Shelf-derived iron inputs drive biological productivity in the southern Drake Passage

H. Dulaiova,[1,2] M. V. Ardelan,[3] P. B. Henderson,[1] and M. A. Charette[1]

[1] In the Southern Ocean near the Antarctic Peninsula, Antarctic Circumpolar Current (ACC) fronts interact with shelf waters facilitating lateral transport of shelf-derived components such as iron into high-nutrient offshore regions. To trace these shelf-derived components and estimate lateral mixing rates of shelf water, we used naturally occurring radium isotopes. Short-lived radium isotopes were used to quantify the rates of shelf water entrainment while $Fe/^{228}Ra$ ratios were used to calculate the Fe flux. In the summer of 2006 we found rapid mixing and significant lateral iron export, namely, a dissolved iron flux of 1.1×10^5 mol d^{-1} and total acid leachable iron flux of 1.1×10^6 mol d^{-1} all of which is transported in the mixed layer from the shelf region offshore. This dissolved iron flux is significant, especially considering that the bloom observed in the offshore region ($0.5-2$ mg chl a m^{-3}) had an iron demand of 1.1 to 4×10^5 mol Fe. Net vertical export fluxes of particulate Fe derived from $^{234}Th/^{238}U$ disequilibrium and $Fe/^{234}Th$ ratios accounted for only about 25% of the dissolved iron flux. On the other hand, vertical upward mixing of iron rich deeper waters provided only 7% of the lateral dissolved iron flux. We found that similarly to other studies in iron-fertilized regions of the Southern Ocean, lateral fluxes overwhelm vertical inputs and vertical export from the water column and support significant phytoplankton blooms in the offshore regions of the Drake Passage.

Citation: Dulaiova, H., M. V. Ardelan, P. B. Henderson, and M. A. Charette (2009), Shelf-derived iron inputs drive biological productivity in the southern Drake Passage, *Global Biogeochem. Cycles*, *23*, GB4014, doi:10.1029/2008GB003406.

1. Introduction

[2] In the Southern Ocean near the Antarctic Peninsula, the geographical distribution of phytoplankton in nutrient-rich waters exhibit large variation with steep concentration gradients [*Mitchell and Holm-Hansen*, 1991; *Holm-Hansen et al.*, 1997; *Barbeau et al.*, 2006]. This variation is due to complex mixing patterns between water masses of various macronutrient and micronutrient contents [*de Baar et al.*, 1995; *Blain et al.*, 2001] as a result of jets, meanders, and eddies associated with topographic features formed as the Antarctic Circumpolar Current (ACC) passes the Drake Passage [*Orsi et al.*, 1995]. The ACC fronts interact with shelf waters near the South Shetland Islands (SSI) and Antarctic Peninsula and may facilitate lateral transport of shelf-derived components such as iron, manganese, silicate, radium and others. *Holm-Hansen et al.* [1997] implied that as a result of shelf water entrainment, shelf-derived

biolimiting trace elements from the Bellinghausen Sea, Bransfield Strait and Weddell Sea mix with high-nutrient low-chlorophyll ACC water enhancing biological productivity north of the SSI (Figure 1).

[3] Intense research concerning the supply of biolimiting trace elements from continental margins and shelves has focused on iron because of its role as an essential element for phytoplankton growth [*Martin and Fitzwater*, 1988]. Since iron limits biological production especially in the HNLC regions [*Martin et al.*, 1991; *Coale et al.*, 1996], rates of iron input may directly control marine productivity in this region of the Southern Ocean. *Berelson et al.* [1996, 2003] suggested that globally, the sedimentary source is at least as large as inputs from mineral dust. Sediment resuspension events [*Luther and Wu*, 1997; *Johnson et al.*, 1997] as well as diffusion of reduced iron from sediments beneath high-productivity regions [*Elrod et al.*, 2004] lead to higher concentrations in coastal and shelf waters. It appears that in the Southern Ocean, shelf sediments supply a significant portion of this micronutrient [*Mitchell and Holm-Hansen*, 1991; *de Baar et al.*, 1995; *Löscher et al.*, 1997; *Blain et al.*, 2001; *Planquette et al.*, 2007] with additional inputs from upwelling, melting sea ice [*Smith et al.*, 2007], atmospheric transport of continental weathering products [*Jickells et al.*, 2005; *Wagener et al.*, 2008], and hydrothermal activity [*Klinkhammer et al.*, 2001].

[1]Department of Marine Chemistry and Geochemistry, Woods Hole Oceanographic Institution, Woods Hole, Massachusetts, USA.
[2]Now at Department of Geology and Geophysics, University of Hawaii, Honolulu, Hawaii, USA.
[3]Department of Chemistry, Norwegian University of Science and Technology, Trondheim, Norway.
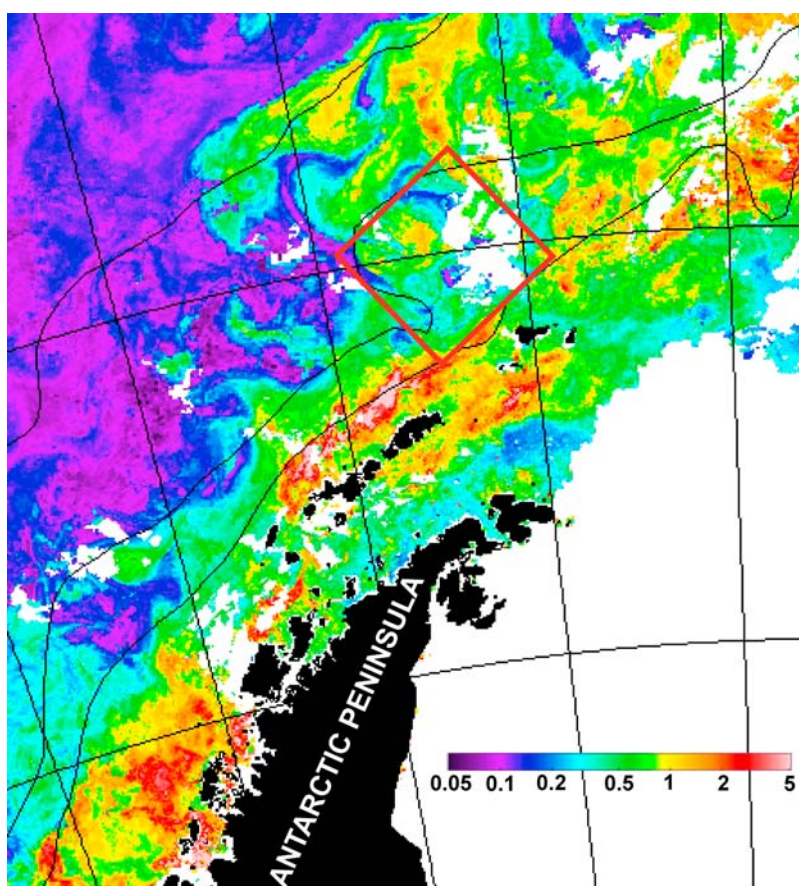
Figure 1. Composite chlorophyll *a* concentration (scale bar in mg m^{-3}) from full-resolution MODIS-Aqua and SeaWiFS data in the southern Drake Passage in the Southern Ocean near the Antarctic Peninsula for the month of February 2006 (B. G. Mitchell, unpublished results, 2006, available at http://spg.ucsd.edu/Satellite_Data). Land masses are black, and white colored areas were covered by clouds. The red rectangle depicts part of the offshore bloom that was the subject of this study. The figure covers the area from latitude 69°S to 57°S and longitude 80°W and 43°W.

However, rapid oxidation and delayed biological response to iron supply, and its unknown cycling within the mixed layer can complicate the identification of the relative importance of different iron supply mechanisms [*Boyd and Mackie*, 2008] and quantification of its lateral and vertical fluxes. Therefore geochemical tracers such as radium and thorium can aid in tracking the horizontal dispersion of shelf-derived iron and its vertical transport via scavenging onto sinking particles.

[4] Shelf-derived components can be traced using the quartet of naturally occurring radium isotopes. Radium is produced by the decay of thorium isotopes (^{227}Th→^{223}Ra, ^{228}Th→^{224}Ra, ^{232}Th→^{228}Ra, and ^{230}Th→^{226}Ra) which are highly particle reactive and are associated with sediments. Through radioactive ingrowth radium isotopes are constantly regenerated in the sediments and enter the ocean via advective (rivers and submarine groundwater discharge [*Li et al.*, 1977; *Moore*, 1996] or diffusive processes [*Geibert*, 2001; *Geibert et al.*, 2002]. Higher radium concentrations are therefore apparent in coastal and shelf areas and near bottom sediments. This enrichment and the fact that the four radium isotopes have different half-lives can be used to identify water masses [e.g., *Zhang et al.*, 2007; *Schmidt and Reyss*, 1996; *Kadko and Muench*, 2005], vertical diffusion coefficients [e.g., *Kaufman et al.*, 1973], and lateral mixing rates [*Moore*, 2000a, 2000b]. Short-lived ^{224}Ra ($T_{1/2}$ = 3.7 days) and ^{223}Ra (11 days) are preferred tracers in nearshore environments with exchange processes on a time scale of 1–3 months [*Moore*, 2000b]. In case of the longer-lived ^{228}Ra ($T_{1/2}$ = 5.8 years), water that has been in contact with land or bottom sediments would carry the "radium signal" for up to 30 years. ^{226}Ra has a half-life of 1600 years and is also a good indicator of upwelled waters [*Hanfland*, 2002; *Zhang et al.*, 2007].

[5] A recent detailed study of the long-lived radium isotope distribution in the Southern Ocean has been published by *Hanfland* [2002]. In the Atlantic sector south of the Polar Front (same as our study site) the author reported elevated surface water ^{226}Ra activities in the Antarctic Surface Water and the Weddell Gyre

(150 dpm.m^{-3}) due to enrichment originating from the extensive shelf region and upwelling. ^{228}Ra concentrations were elevated (>20 dpm.m^{-3}) only in coastal and shelf regions with very low to no detectable activities in the ACC ($\leq$0.2 dpm.m^{-3}). The author showed that ^{228}Ra has an excellent potential as tracer of shelf signals into the open South Atlantic, but did not have supporting offshore flux estimates. Nevertheless their study showed that oceanic fronts act as an effective transport mechanism of shelf components into the productive regions of the ACC.

[6] Short-lived radium isotopes in the Southern Ocean have been applied by *Charette et al.* [2007] as tracers of lateral transport rates of shelf-derived iron around the Crozet Islands. They observed that lateral inputs of Fe from the Crozet Plateau dominated over vertical sources. *Smith et al.* [2007] used short-lived radium isotopes to trace debris sediment material released from free-drifting icebergs. The authors found rapid melting and dispersion of entrained terrigenous material, which they assumed to be a likely contributor to elevated iron concentrations in the vicinity of our study area near the South Shetland Islands.

[7] Radium in the surface layer is not subject to chemical or biological uptake. On the other hand, iron is removed from the water column by scavenging onto sinking particles, which may regulate the intensity and duration of an iron-fertilized bloom. Quantitative estimates of scavenging rates of Fe can be made using thorium (Th) which is a metal with similar abiological properties to Fe [*Parekh et al.*, 2004]. These authors suggest that similarly to Th, Fe is scavenged on particles and may even be released back to the water column via remineralization. *Weinstein and Moran* [2005] studied iron fluxes from ^{234}Th depletion profiles in the Labrador Sea and found that the Fe/Th ratios were not correlated to particle size.

[8] The goal of this study was to determine the transport mechanism and flux of iron in the shelf region of the Antarctic Peninsula using radium isotopes. Short-lived radium isotopes were used to quantify the rates of water transport while Fe/^{228}Ra ratios were used to calculate the Fe flux. Export fluxes of Fe, derived from ^{234}Th/^{238}U disequilibrium, are compared with the shelf-derived inputs in an attempt to create a Fe mass balance for the upper water column. Last, the magnitude of the Fe flux was weighed against its potential for sustaining the offshore blooms in this region.

2. Methods

[9] Samples for radium isotope analyses were collected aboard the *RV Yuzhmorgeologiya* during the Antarctic Marine Living Resources (AMLR) 2006 cruise in the Southern Ocean between 14 January and 8 February 2006 (Figures 1 and 2). We focused our sampling on the area of South Shetland Islands (SSI), Bransfield Strait (BS) and the vicinity of Elephant Island (EI). We collected large volume surface seawater samples (550–750 L) from the ship's seawater intake. To confirm that the seawater intake was well flushed and not contaminated by thorium isotopes and the pipes were not contributing additional Ra into the pumped seawater [*Charette et al.*, 2007], we compared samples collected this way to water collected from the CTD from 5 m depth on our first sampling station. At each station from then on the water was pumped from 5 m depth at a rate of 60 L min^{-1}. We filled several 200 L containers to the desired volume. At each station we collected subsamples from the containers for salinity analysis. Salinity samples were analyzed by a Guideline AutoSal instrument. The water was then passed through a single column filled with MnO$_2$-coated acrylic fiber using submersible pumps at a flow rate of $\leq$1 L min^{-1} (radium adsorption efficiency 99%). Several 60 to 100 L samples were collected on land on 3 islands of the SSI into plastic containers. These were passed through MnO$_2$-coated fibers by controlled gravity flow. After passing the seawater through the columns we washed the Mn fiber with Ra-free water and dried the fiber using pressurized air. The radium was measured immediately on board using a delayed coincidence counter system [*Moore and Arnold*, 1996]. We had a system with two counters that were recalibrated against a NIST traceable standard on the ship. Because the large-volume samples had high levels of ^{226}Ra, ^{222}Rn built up relatively quickly in the closed system producing high background and elevated chance coincidence counts in the 220 window. The fibers were therefore only counted for 2–3 h after which we disconnected the column from the system and purged it for about 10 min. Then we flushed the system with helium and restarted the counting. The counts collected during the two counting cycles and the counting times were then added together and treated as one measurement. Fibers were recounted again within 7 to 10 days for ^{223}Ra, after 1 month since sample collection for ^{228}Th, and after 3 months for ^{227}Ac. The samples were then ashed, sealed into vials, and counted for ^{226}Ra and ^{228}Ra on a well-type germanium gamma-spectrometer. All ^{224}Ra reported hereafter are unsupported activities measured in excess of its ^{228}Th parent. We do not report the ^{223}Ra and ^{227}Ac values as these had very high (>30%) measurement uncertainties and were not used for mixing rate calculations.

[10] At each station a CTD-instrumented rosette was deployed down to 750 m (or within few meters of the bottom) with data being recorded on both the down and up casts. Thorium-234 was measured at selected stations to cover a depth between 0 to 750 m (or shallower above the shelf). Profiles of total ^{234}Th were collected from 4 L samples from CTD casts and analyzed using methods outlined by *Buesseler et al.* [1998]. Samples for particulate C/^{234}Th ratios were collected by battery-powered, large-volume in situ pumps (McLane Laboratories) by passing 300 L of water at the predetermined depths (20 and 100 m) sequentially through 142 mm diameter filters mounted in a baffled filter housing at ~8 L min^{-1}. The first filter was a polyester screen with a nominal mesh size of 54 μm, followed by a quartz filter (QMA) with a 1 μm nominal pore size. All thorium fractions were counted on gas flow proportional beta counters manufactured by Riso National Laboratories [*Buesseler et al.*, 1998]. Aliquots of the same filters were analyzed for particulate organic carbon by fuming the samples with HCL to remove carbonate followed by analysis with a Thermo Quest Flash EA 1112 CHN analyzer.
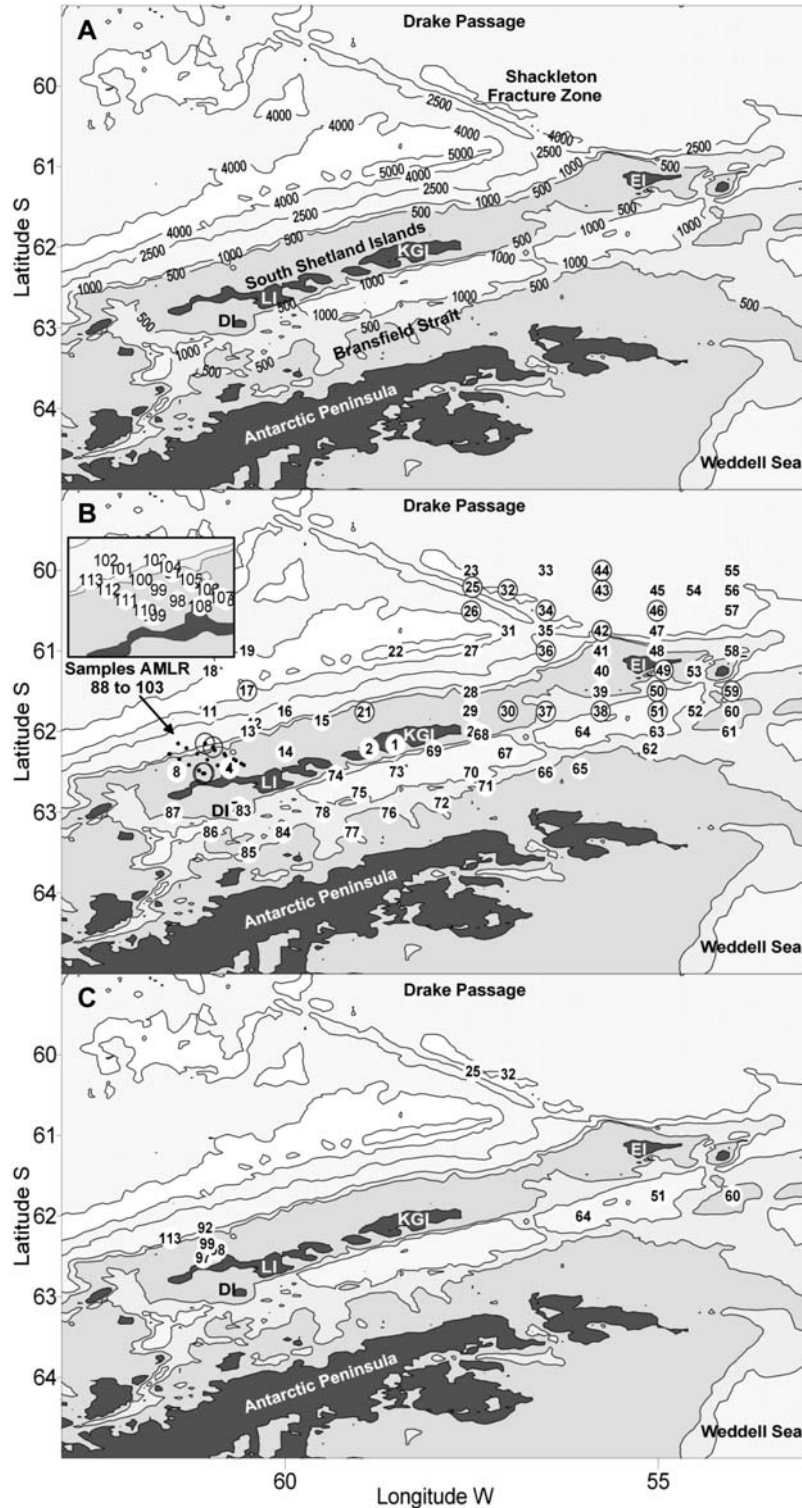
Figure 2. (a) Detailed bathymetric map of the southern Drake Passage near the Antarctic Peninsula. Landmasses are black, and the shaded regions with depth isoplets depict 500, 1000, 2500, 4000, and 5000 m isobars. Abbreviations are as follows: EI, Elephant Island; KGI, King George Island; LI, Livingston Island; DI, Deception Island. (b) Radium-sampling locations are indicated by their sample ID based on Table 1. Thorium samples were only collected at stations that are circled with black. The inset shows the detailed nearshore sampling transects (samples 88 to 113). These were used for the LI transect calculation in Figure 6. (c) Iron-sampling locations indicated by sample ID based on Table 1.

Table 1. Surface Water Samples[a]

Sample ID	AMLR ID	Depth	Latitude	Longitude	Salinity	^{224}Ra	^{226}Ra	^{228}Ra	^{228}Th	DFe	TalFe
1	KGI[b]	<1	−62.1626	−58.5224	33.872	12.3 ± 0.6	203.1 ± 1.9	14.2 ± 2.4	2.3 ± 0.5		
2	KGI[b]	<1	−62.2113	−58.8725	34.102	3.6 ± 0.7	185.9 ± 1.7	7.2 ± 1.6	2.6 ± 0.7		
3	LI[b]	<1	−62.4529	−60.7454	33.971	7.3 ± 0.1	280.1 ± 3.5	20.4 ± 3.2	1.8 ± 0.7		
4	LI[b]	<1	−62.4529	−60.7454	29.160	5.9 ± 3.1	138.7 ± 2.1	12.3 ± 2.8	1.5 ± 0.5		
8	17−11	128	−62.4985	−61.4518	34.129	5.9 ± 1.1	203.9 ± 4.7	14.6 ± 4.2	1.0 ± 0.5		
11	16−08	3196	−61.7488	−61.0057	34.168	0.1 ± 0.2	179.4 ± 1.5	5.3 ± 1.1	1.4 ± 0.4		
12		2200	−61.8986	−60.4177	34.111	1.8 ± 0.3	138.3 ± 1.3	2.9 ± 1.2	1.1 ± 0.2		
13	15−09	1443	−61.9959	−60.4980	34.194	0.8 ± 0.2	150.6 ± 1.1	6.1 ± 1.0	1.0 ± 0.3		
14	14−10	2006	−62.2473	−59.9963	34.200	3.2 ± 0.4	208.9 ± 2.0	4.7 ± 1.1	1.2 ± 0.3		
15	13−09	173	−61.8612	−59.5054	34.181	2.6 ± 0.3	140.2 ± 1.5	5.9 ± 1.3	1.2 ± 0.3		
16	14−08	1590	−61.7475	−60.0041	34.150	1.0 ± 0.3	213.6 ± 1.9	4.6 ± 1.1	1.0 ± 0.2		
17	15−07	4022	−61.4917	−60.5103	33.820	1.2 ± 0.2	121.7 ± 0.7	2.0 ± 0.5	0.2 ± 0.1		
18	16−06	3989	−61.2479	−61.0042	33.948	0.6 ± 0.2	154.3 ± 1.5	4.2 ± 1.6	0.2 ± 0.1		
19	15−05	3708	−60.9955	−60.5072	34.188	0.4 ± 0.1	180.1 ± 1.5	3.6 ± 1.0	0.2 ± 0.1		
20	13−07	3074	−61.9992	−57.4585	34.297	1.9 ± 0.3	154.4 ± 1.6	3.5 ± 1.3	0.6 ± 0.3		
21	12−08	316	−61.7553	−58.9356	34.158	1.3 ± 0.2	147.2 ± 0.9	6.5 ± 0.9	1.1 ± 0.3		
22	11−05	5084	−61.0052	−58.5166	33.921	1.2 ± 0.2	171.9 ± 1.5	5.5 ± 1.3	0.6 ± 0.2		
23	11−03[c]	3730	−60.0035	−57.5008	34.014	1.1 ± 0.2	147.2 ± 1.1	3.9 ± 1.0	0.7 ± 0.2		
24	09−01[c]	3758	−60.2075	−57.4851	34.106	1.3 ± 0.2	143.2 ± 1.1	2.1 ± 0.8	0.4 ± 0.2		
25	09−02[c]	3284	−60.2075	−57.4851	33.885	1.0 ± 0.1	129.6 ± 0.7	1.9 ± 0.6	0.1 ± 0.1	0.17	0.80
26	09−03[c]	3579	−60.5085	−57.5028	33.826	0.9 ± 0.2	125.7 ± 1.1	1.7 ± 0.9	0.2 ± 0.1		
27	09−05[c]	3937	−60.9997	−57.4986	33.899	1.1 ± 0.2	149.9 ± 1.4	3.1 ± 1.4	0.6 ± 0.2		
28	09−07	613	−61.5087	−57.5098	34.331	1.5 ± 0.3	114.3 ± 1.1	3.5 ± 1.4	1.5 ± 0.5		
29	09−08	350	−61.7424	−57.5143	34.074	0.8 ± 0.3	161.7 ± 1.2	5.8 ± 1.0	0.7 ± 0.2		
30	08−08	411	−61.7475	−57.0070	34.119	1.2 ± 0.2	167.8 ± 1.0	6.8 ± 1.0	1.6 ± 0.4		
31	08−04[c]	3519	−60.7514	−56.9977	33.862	1.0 ± 0.2	127.7 ± 0.8	2.4 ± 0.6	0.3 ± 0.1		
32	08−02[c]	4079	−60.2439	−57.0102	33.891	1.2 ± 0.1	126.3 ± 0.6	2.1 ± 0.5	0.2 ± 0.1	0.12	0.45
33	07−01[c]	3579	−60.0002	−56.4998	33.986	0.9 ± 0.2	148.8 ± 1.0	4.6 ± 1.2	0.4 ± 0.1		
34	07−03[c]	3799	−60.4989	−56.5007	33.827	0.8 ± 0.2	128.7 ± 0.9	2.0 ± 0.6	0.4 ± 0.1		
35	07−04[c]	2524	−60.7455	−56.5031	33.879	0.7 ± 0.2	142.2 ± 0.8	2.4 ± 0.5	0.8 ± 0.3		
36	07−05[c]	2103	−60.9980	−56.4990	33.868	0.7 ± 0.2	137.6 ± 3.1	<dl	1.0 ± 0.3		
37	07−08	531	−61.7489	−56.4990	33.984	1.4 ± 0.2	157.2 ± 1.8	8.7 ± 1.5	1.1 ± 0.2		
38	05.5−08[c]	1288	−61.7465	−55.7629	34.358	1.6 ± 0.2	167.1 ± 0.9	6.7 ± 0.8	1.9 ± 0.4		
39	05.5−07[c]	211	−61.5070	−55.7666	34.067	2.1 ± 0.2	158.5 ± 2.7	6.4 ± 2.0	0.8 ± 0.3		
40	05.5−06[c]	124	−61.2473	−55.7483	34.175	1.1 ± 0.2	124.1 ± 0.8	6.2 ± 0.8	1.2 ± 0.3		
41	05.5−05[c]	159	−60.9988	−55.7546	34.284	1.0 ± 0.2	130.2 ± 0.8	6.1 ± 0.8	1.0 ± 0.2		
42	05.5−04[c]	1516	−60.7494	−55.7501	34.010	1.2 ± 0.3	128.0 ± 1.1	6.2 ± 1.1	1.0 ± 0.3		
43	05.5−02[c]	3544	−60.2498	−55.7446	33.877	0.5 ± 0.3	147.3 ± 1.1	3.0 ± 0.9	0.5 ± 0.2		
44	05.5−01[c]	1523	−60.0017	−55.7483	34.283	0.4 ± 0.1	131.2 ± 0.6	2.2 ± 0.5	0.6 ± 0.2		
45	04−02	3289	−60.2499	−55.0015	33.913	1.1 ± 0.2	161.5 ± 0.9	4.0 ± 0.8	0.9 ± 0.2		
46	04−03[c]	3353	−60.4997	−55.0085	33.965	0.4 ± 0.2	160.3 ± 1.0	3.8 ± 0.7	1.3 ± 0.3		
47	04−04[c]	3126	−60.7501	−55.0067	34.108	1.0 ± 0.2	156.3 ± 1.0	4.5 ± 0.8	1.1 ± 0.4		
48	04−05	520	−60.9980	−55.0085	34.411	2.5 ± 0.3	163.9 ± 1.1	6.6 ± 1.1	1.1 ± 0.2		
49	04−06	109	−61.2404	−54.9207	34.194	4.1 ± 0.3	160.8 ± 1.0	5.1 ± 0.8	2.0 ± 0.5		
50	04−07[c]	844	−61.4983	−55.0085	34.129	1.8 ± 0.3	174.1 ± 0.8	6.0 ± 0.7	1.3 ± 0.4		
51	04−08[c]	2012	−61.7497	−54.9976	34.765	1.9 ± 0.3	166.9 ± 0.8	10.0 ± 1.5	1.3 ± 0.3	0.66	2.17
52	03−08[c]	670	−61.7460	−54.4955	34.306	1.9 ± 0.3	148.9 ± 1.0	4.5 ± 1.0	1.1 ± 0.2		
53	03−06[c]	579	−61.2533	−54.5068	34.052	1.0 ± 0.2	129.6 ± 0.9	6.1 ± 0.9	0.9 ± 0.3		
54	03−02	2988	−60.2496	−54.5142	33.921	1.2 ± 0.2	160.7 ± 1.0	3.8 ± 0.9	0.5 ± 0.2		
55	02−01	2972	−60.0025	−53.9971	33.865	0.5 ± 0.1	127.1 ± 0.9	3.0 ± 0.8	0.5 ± 0.2		
56	02−02	2578	−60.2478	−53.9978	33.856	0.5 ± 0.1	130.8 ± 1.1	3.0 ± 0.8	0.5 ± 0.1		
57	02−03	2970	−60.4990	−54.0002	33.885	1.3 ± 0.2	144.0 ± 1.0	4.6 ± 0.9	0.3 ± 0.1		
58	02−05[c]	2578	−60.9980	−54.0015	34.235	2.2 ± 0.3	181.4 ± 1.1	5.4 ± 0.9	1.0 ± 0.3		
59	02−07[c]	741	−61.5009	−54.0051	34.346	1.4 ± 0.2	150.8 ± 1.1	5.9 ± 1.0	1.5 ± 0.4		
60	02−08[c]	328	−61.7488	−53.9990	34.491	2.3 ± 0.3	160.5 ± 1.0	5.2 ± 0.9	1.3 ± 0.2	0.6	10.0
61	02−09[c]	549	−61.9979	−54.0330	34.361	1.7 ± 0.3	188.8 ± 1.8	7.1 ± 1.4	1.7 ± 0.4		
62	04−10[c]	540	−62.2142	−55.1001	34.365	2.8 ± 0.3	157.1 ± 1.0	9.4 ± 0.9	1.5 ± 0.5		
63	04−09[c]	1325	−62.0023	−55.0056	34.300	1.6 ± 0.2	152.6 ± 0.7	7.8 ± 0.7	1.2 ± 0.3		
64	06−09[c]	2150	−62.0022	−56.0039	34.342	0.9 ± 0.2	118.2 ± 1.0	6.3 ± 1.0	0.7 ± 0.3	0.44	1.86
65	06−11	378	−62.4578	−56.0378	34.390	2.8 ± 0.3	170.9 ± 1.1	11.7 ± 1.2	2.2 ± 0.7		
66	07−11	357	−62.5047	−56.5023	34.400	2.0 ± 0.3	170.0 ± 1.2	9.4 ± 1.1	1.9 ± 0.5		
67	08−10	1580	−62.2667	−57.0413	34.335	2.0 ± 0.3	151.1 ± 0.9	7.0 ± 0.9	1.0 ± 0.2		
68	09−09	248	−62.0368	−57.3633	34.486	0.9 ± 0.3	162.4 ± 1.2	9.4 ± 1.3	1.8 ± 0.4		
69	10−10	1451	−62.2410	−57.9997	33.858	0.7 ± 0.2	139.2 ± 0.6	7.5 ± 0.7	1.2 ± 0.4		
70	09−11	1485	−62.5020	−57.4995	34.324	1.5 ± 0.2	154.6 ± 1.1	6.9 ± 1.0	1.0 ± 0.3		
71	8−12	563	−62.6733	−57.3042	34.314	3.2 ± 0.4	167.0 ± 1.0	9.4 ± 0.9	1.9 ± 0.3		
72	09−13	431	−62.8848	−57.8972	34.330	1.6 ± 0.3	165.1 ± 1.1	6.2 ± 0.9	1.7 ± 0.5		
73	11−11	1641	−62.4972	−58.5004	34.303	1.1 ± 0.2	154.0 ± 1.0	9.7 ± 1.0	1.4 ± 0.4		
74	13−11	855	−62.5450	−59.3213	33.984	1.0 ± 0.2	125.1 ± 0.8	11.8 ± 1.2	0.7 ± 0.1		
75	12−12	1450	−62.7515	−59.0039	34.506	2.1 ± 0.3	125.5 ± 1.2	6.5 ± 1.2	0.9 ± 0.2		
76	11−13	311	−63.0046	−58.6035	34.434	1.5 ± 0.3	129.4 ± 1.0	5.1 ± 0.9	1.7 ± 0.5		

Table 1. (continued)

Sample ID	AMLR ID	Depth	Latitude	Longitude	Salinity	^{224}Ra	^{226}Ra	^{228}Ra	^{228}Th	DFe	TalFe
77	12−14	149	−63.2430	−59.0959	34.407	2.1 ± 0.3	191.8 ± 1.1	9.0 ± 1.1	2.4 ± 0.5		
78	14−12	913	−62.9997	−59.4946	34.020	2.8 ± 0.3	177.8 ± 1.1	8.5 ± 1.2	1.1 ± 0.2		
79	DI	106	−62.9355	−60.6205	33.873	1.8 ± 0.2	138.7 ± 1.0	6.9 ± 1.0	0.7 ± 0.2		
83	DI[b]	<1	−62.9803	−60.5553		13.2 ± 1.7	56.5 ± 2.2	17.8 ± 4.0	1.9 ± 0.9		
84	14−14	845	−63.2463	−60.0280	34.408	1.9 ± 0.3	133.1 ± 0.9	6.2 ± 0.9	1.1 ± 0.3		
85	15−15	544	−63.4959	−60.4871	34.331	1.1 ± 0.3	159.7 ± 0.9	9.4 ± 1.1	1.7 ± 0.4		
86	16−14	833	−63.2431	−60.9961	33.447	2.8 ± 0.3	172.4 ± 1.3	10.8 ± 1.3	0.8 ± 0.3		
87	17−13	475	−63.0014	−61.5015	34.114	1.5 ± 0.2	117.5 ± 0.9	3.4 ± 0.8	0.5 ± 0.2		
88	Y8−5[d]	311	−62.4145	−60.551	34.213	1.8 ± 0.2	170.8 ± 0.9	5.7 ± 0.9	0.9 ± 0.2		
89	Y8−4[d]	339	−62.3563	−60.6583	34.209	0.9 ± 0.2	203.6 ± 1.4	6.0 ± 1.3	1.7 ± 0.3		
90	Y8−3[d]	269	−62.2965	−60.8011	34.150	1.9 ± 0.2	134.4 ± 0.9	5.2 ± 0.9	0.7 ± 0.2		
91	Y8−2[d]	205	−62.2283	−60.9437	34.010	1.5 ± 0.2	134.7 ± 0.9	4.7 ± 0.9	0.7 ± 0.2		
92	Y8−1[d]	1070	−62.1453	−61.0743	33.985	0.9 ± 0.1	124.3 ± 0.7	4.2 ± 0.6	0.8 ± 0.2	0.36	1.4
93	Y2−1[d]	1200	−62.2773	−61.5562	34.071	1.4 ± 0.2	156.4 ± 1.1	6.9 ± 1.0	0.9 ± 0.2		
94	Y2−2[d]	430	−62.3413	−61.4204	34.142	1.1 ± 0.2	127.8 ± 0.8	4.6 ± 0.8	0.9 ± 0.2		
95	Y2−3[d]	401	−62.4101	−61.2898	34.215	1.4 ± 0.2	171.3 ± 1.3	5.0 ± 1.0	1.2 ± 0.2		
96	Y2−4[d]	394	−62.4797	−61.1544	34.870	1.6 ± 0.2	135.1 ± 0.9	3.3 ± 0.8	0.8 ± 0.2		
97	Y2−5[d]	338	−62.5175	−61.1023	34.119	4.4 ± 0.3	162.5 ± 1.1	7.1 ± 1.0	0.9 ± 0.2	1.61	101.7
98	Y5−5[d]	90	−62.4188	−60.9068	34.168	3.4 ± 0.2	137.1 ± 0.8	6.1 ± 0.8	0.9 ± 0.2	1.25	
99	Y5−3[d]	140	−62.3458	−61.0457	34.195	0.8 ± 0.2	153.9 ± 1.0	3.6 ± 0.7	1.7 ± 0.3		
100	Y5−2[d]	282	−62.275	−61.181	34.151	0.9 ± 0.2	166.5 ± 1.4	6.6 ± 1.2	1.4 ± 0.3		
101	Y5−1[d]	1198	−62.203	−61.3239	33.985	1.9 ± 0.2	136.0 ± 0.9	3.8 ± 0.9	0.4 ± 0.2		
102	Y5−0[d]	1869	−62.1452	−61.4348	34.034	1.4 ± 0.2	151.9 ± 1.2	5.2 ± 1.1	0.9 ± 0.2		
103	Y8−1[d]	1115	−62.1428	−61.0731	34.260	1.4 ± 0.2	158.8 ± 1.0	5.7 ± 0.9	1.2 ± 0.2		
104	Y8-1-2[d]	195	−62.1892	−60.969	34.156	1.8 ± 0.2	146.9 ± 0.9	5.3 ± 0.8	0.8 ± 0.2		
105	Y8-2-3[d]	260	−62.2739	−60.8143	33.913	1.6 ± 0.2	145.7 ± 1.0	4.2 ± 0.9	1.3 ± 0.2		
106	Y8-3-4[d]	331	−62.3418	−60.689	34.186	1.5 ± 0.2	185.9 ± 1.2	5.9 ± 1.1	1.1 ± 0.2		
107	Y8-4-5[d]	320	−62.3956	−60.587	34.262	1.7 ± 0.2	125.2 ± 0.8	4.7 ± 0.8	0.8 ± 0.2		
108	LI[d]	90	−62.4546	−60.7441	34.731	2.7 ± 0.2	124.1 ± 0.9	3.5 ± 0.8	0.9 ± 0.2		
109	Y2−5[d]	340	−62.5155	−61.0827	34.168	2.6 ± 0.2	175.7 ± 1.2	6.7 ± 1.2	1.5 ± 0.3		
110	Y2−4[d]	395	−62.4803	−61.1545	34.169	2.2 ± 0.2	138.0 ± 1.0	5.5 ± 1.0	0.6 ± 0.2		
111	Y2−3[d]	400	−62.4111	−61.2906	34.087	1.2 ± 0.2	161.6 ± 1.1	4.2 ± 0.9	0.9 ± 0.2		
112	Y2−2[d]	430	−62.3415	−61.4168	34.203	1.5 ± 0.2	139.2 ± 0.9	5.1 ± 0.8	0.8 ± 0.2		
113	Y2−1[d]	1198	−62.2763	−61.5445	34.061	0.7 ± 0.2	203.9 ± 1.5	7.9 ± 1.4	1.3 ± 0.3	0.42	3.07

[a]Collected at 5 m depth (or shallower for coastal samples) with sampling coordinates, salinity, ^{224}Ra, ^{226}Ra, ^{228}Ra, and ^{228}Th activities (dpm m^{-3}), dissolved acid leachable iron (DFe = 0.2 μm filtered, acidified, nM), and total acid leachable iron (TalFe = dissolved form plus labile particulate fraction released at pH 1.7–1.8, nM) from the surface 50 m (Ardelan et al., manuscript in preparation, 2009). Also indicated is the depth of the water column at each station. ^{224}Ra is unsupported, i.e., in excess of that supported by the ^{228}Ra-^{228}Th pair, where total ^{224}Ra can be derived as the sum of unsupported ^{224}Ra and ^{228}Th activities from Table 1. Sample IDs correspond to those shown in Figure 2, AMLR ID is station identification based on the NOAA's AMLR program or the name of the island where the nearshore sample was collected (KGI, King George Island; LI, Livingston Island; DI, Deception Island).
[b]Coastal samples collected at the shoreline or in nearshore areas.
[c]Samples included in the EI transect.
[d]Samples included in the LI transect.

[11] Iron samples were collected with Teflon-lined GO-FLO bottles deployed with trace metal clean polymer 1/4″ Sta-Set X linen (New England ropes) line. All sample preparation was conducted in a HEPA-filtered Class 100 laminar flow clean area. Dissolved iron (DFe) samples were filtered by an acid washed inline filter (0.4 μm pore size pre filter and 0.2 μm pore size filter, Sartobran-Sartorious) immediately after sample collection. DFe was operationally defined by 0.2 μm nominal pore size; thus, it includes colloidal Fe. Both DFe and total acid leachable iron (TalFe) samples have been acidified to pH 1.7–1.8 with 15.4 M ultrapure(UP) HNO$_3$ (optima grade, Sigma). All acidified filtrate samples were stored for at least 7–8 months before processing. Preconcentration of DFe and TalFe from seawater was carried out by a combination of Chelex-100 (Na$^+$ form, 100–200 mesh size, Bio-Rad) batch [*Baffi and Cardinale*, 1990; *Grotti et al.* 2001] and column techniques [*Öztürk*, 1995; *Öztürk et al.* 2002; M. V. Ardelan et al., Natural iron enrichment around the Antarctic Peninsula in the Southern Ocean, manuscript in preparation, 2009, hereafter Ardelan et al., manuscript in preparation, 2009]. The preconcentra-

tion factor was 100. The final measurement of metals had been performed by HR-ICP-MS (Thermo Finnigan Element) at the Department of Chemistry of Norwegian University of Science and Technology.

3. Results

[12] Our cruise track covered an area of about 450 × 450 km of the Drake Passage and the vicinity of the SSI (Figures 2b and 2c). We collected representative samples in different geographical areas such as the ACC in Drake Passage, shelf water around the EI and LI, and BS. The ACC in the Drake Passage is characterized by warm (>3°C), low-salinity (σ_θ = 26.8) surface water sitting on top of cooler winter water (−1°C). Shelf water in the EI region is shallow and originates from the BS and Weddell Sea; the surface 200 m has a higher density (σ_θ = 27.2–27.4) and a distinct mixed layer of about 50 m. The Weddell water is cold (<0°C), dense, weakly stratified and shows little vertical structure.
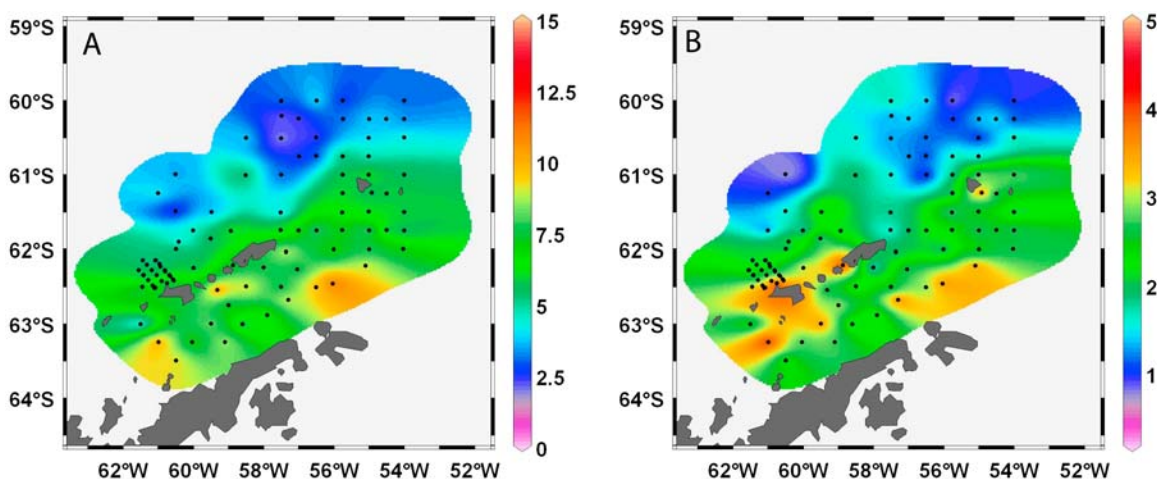
Figure 3. (a) The ^{228}Ra and (b) excess ^{224}Ra distribution in the surface water. Contours are plotted on the basis of the measured activities (dpm m^{-3}), which are indicated on the scale bars. The black circles represent sampling sites. Plots were created in Ocean Data View (R. Schlitzer, 2006, available at http://odv.awi.de).

[13] Radium isotopes were elevated in the mixed surface layer above the shelf, the BS, and in Weddell Sea shelf water. In the nearshore regions around the SSI we found 8–17 dpm m^{-3} ^{224}Ra, 10–20 dpm m^{-3} ^{228}Ra, and 200–290 dpm m^{-3} ^{226}Ra (sample ID 1–4, 83 and 108 in Table 1 and Figure 2). The concentration contours of surface water radium roughly matched the bathymetry (Figures 2a and 3), with higher activities above the shelf and around land-masses. Shelf water had 2–4 dpm m^{-3} ^{224}Ra, 5–10 dpm m^{-3} ^{228}Ra, 150–200 dpm m^{-3} ^{226}Ra. The Drake Passage and ACC water had no excess ^{223}Ra and ^{224}Ra, ^{228}Ra was below detection limit, and ^{226}Ra concentrations were ~130 dpm m^{-3}. In the BS we collected one sample in the vicinity of a free-drifting iceberg which had elevated radium and lower salinity (sample ID 86). No other open water samples were collected near icebergs. We observed relatively high ^{224}Ra in excess of its parent ^{228}Th in the offshore region at >200 km NW of EI (sample ID 35, 39, 40; Table 1).

[14] We also sampled coastal water and submarine springs on Deception Island (sample ID 79, 83), King George Island (sample ID 1, 2), and on Livingston Island (sample ID 3, 4, 108) where the submarine springs were significantly enriched in radium (~17 dpm m^{-3} ^{224}Ra and ~18 dpm m^{-3} ^{228}Ra).

[15] Dissolved iron (DFe) concentrations averaged in the 50 m surface mixed layer were elevated in the coastal and shelf regions >1 nM and much lower, <0.2 nM offshore about 100–150 km north of SSI and EI. Total iron (TalFe = total acid leachable iron from unfiltered samples) had the same trend as dissolved iron with concentrations as high as 100 nM nearshore, up to 10 nM in the shelf region, and as low as 0.4–0.6 nM offshore. These findings were in good agreement with other published measurements made in this region during austral summer [Hopkinson et al., 2007].

[16] The particle reactive ^{234}Th profiles in several stations showed depletion in comparison to its conservative parent ^{238}U and in many cases we found remineralization at depths below 100 m. The ^{234}Th/^{238}U profiles and corresponding carbon fluxes are discussed by M. A. Charette et al. (Carbon fluxes via Th/U, manuscript in preparation, 2009, hereafter Charette et al., manuscript in preparation, 2009).

4. Discussion

[17] Chlorophyll concentrations in the offshore region off EI are above 2 mg m^{-3} and cover an area of 250 × 250 km
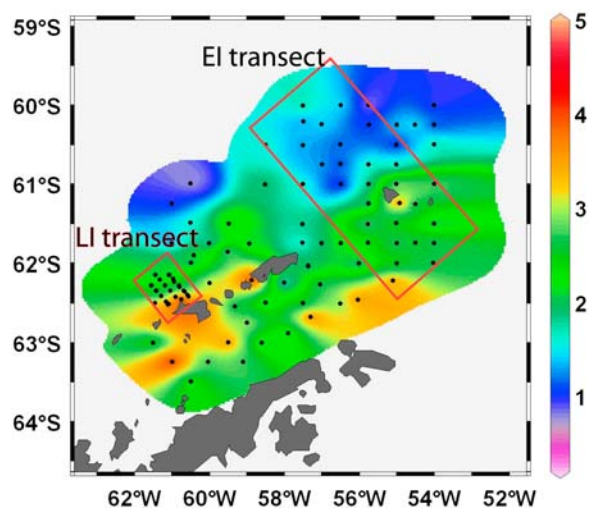

Figure 4. Cross-shelf transects (left) off Livingston Island (see also Figure 2b, inset) and (right) near Elephant Island, which were the focus of our radium and iron flux study. The transects, composed of all data within the red rectangles, are plotted over the ^{224}Ra activity contours. The bathymetry of the region is shown in Figure 2a, and radium trends plotted over distance are shown in Figures 5 and 6. These data are also identified in the footnotes of Table 1 as LI transect and EI transect. Plots were created in Ocean Data View.
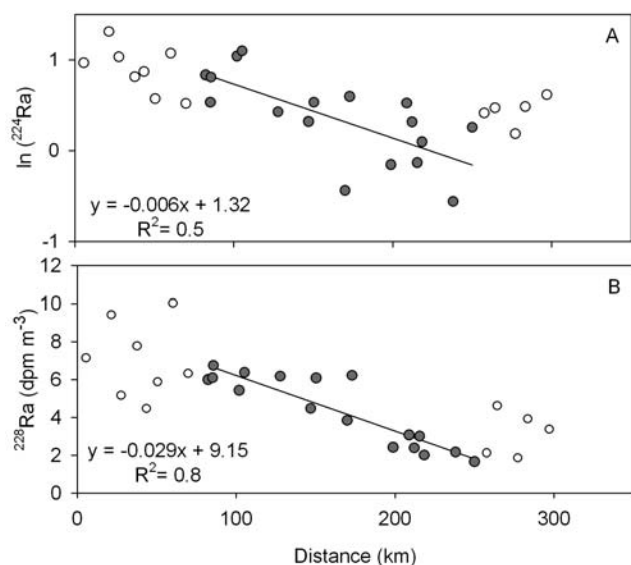
Figure 5. (a) The $\ln^{224}$Ra profile and (b) linear ^{228}Ra distribution on the Elephant Island transect. The solid symbols represent samples included in the calculation of the trendline between the shelf edge and offshore region before the $\ln^{224}$Ra and ^{228}Ra slope changes. Open symbols represent shelf and offshore samples that were excluded from the trend calculation. The shelf extends to about 100 km on the transect (open symbols). The slopes are indicated for each trendline for the solid circles only.

(Figure 1). Such blooms require a significant iron supply and although from the available data we are not able to create a complete iron balance, we are able to estimate some of its major source and loss terms. In sections 4.1 and 4.2 we derive horizontal mixing rates and use Ra/Fe ratios to estimate lateral iron fluxes from the shelf to offshore regions. Our study area covers the bloom region only partially (identified by the red rectangle in Figure 1), namely the 150 km offshore part of the 150 km wide EI transect (Figure 4). In order to assess whether there is sufficient iron remaining in the water column to support the observed biological production, we also estimate net removal rates of this Fe from the dissolved iron pool and calculate vertical particulate iron removal using Fe/Th ratios. Although the processes considered in this study are far from complete, these estimates allow us to demonstrate that lateral iron inputs from the shelf are sufficient to fuel large-scale phytoplankton blooms downstream of the SSI.

4.1. Horizontal Mixing Rates Between the Shelf and Drake Passage

[18] Water near land and above the shelf was enriched in all four radium isotopes. The presence of excess short-lived isotopes is an indication that the water mass is supplied with significant levels of shelf-derived components at a rate at which elevated radium concentrations persist despite their radioactive decay (half-lives of 3.7 and 11 days). From the two short-lived isotopes, ^{224}Ra has a higher natural abun-

dance and was therefore measured with better accuracy (5– 10% relative error). The ^{223}Ra values have >30% relative error due to low count rates and are not used for flux calculations in this study. From the long-lived isotopes we use ^{228}Ra because its sources to the region include the shelf and coastline but no offshore sources, as opposed to ^{226}Ra which is additionally enriched by upwelling and has significant offshore concentrations.

[19] In order to establish horizontal fluxes of shelf-derived components into the Drake Passage, we examined two transects, one across a 150 km wide shelf region near EI and a transect perpendicular to Livingston Island (LI) (Figure 4). We chose to compare these two contrasting regions based on chlorophyll *a* measurements offshore of these two transect where the LI transect does not seem to be as efficient in offshore iron transport as the EI region. On the EI transect we used data collected on a 150 km wide transect (Figure 5) and the ^{224}Ra and ^{228}Ra values were rather scattered. However, taking into account all data on the 150 km wide transect in our calculation has the advantage that we smooth out small-scale disturbances (eddies) in the radium profile and get an estimate of the net transport from the full width of the shelf. Despite the scatter, ^{224}Ra was relatively constant above the EI shelf (average = 2.5 dpm m^{-3}) and decreased to <0.5 dpm m^{-3} at a distance of 150 km from the shelf edge (= 250 km on the EI transect, Figure 5). The end of the transect (>250 km) had elevated ^{224}Ra and ^{228}Ra values, which would require a very fast offshore transport of coastal waters without significant dilution with low-radium offshore waters. A recent formation of a large eddy entraining shelf water or shelf streamers similar to those observed by *Rasmussen* [2003] could be responsible for quick lateral transport preserving coastal ^{224}Ra/^{228}Ra ratios. Alternatively, high particulate ^{228}Th,
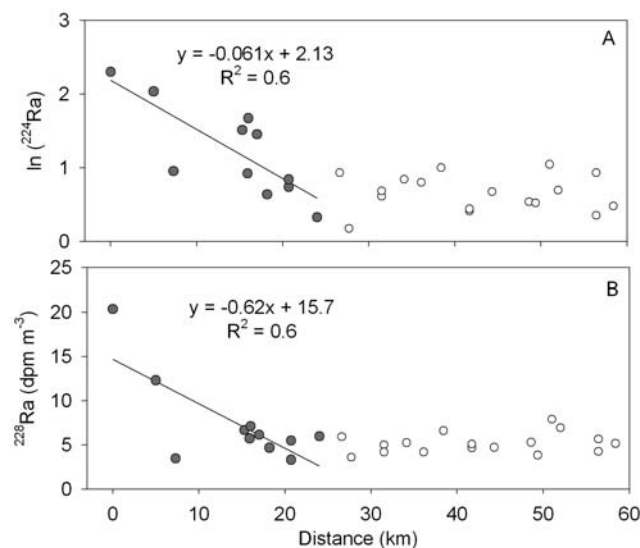

Figure 6. (a) The $\ln^{224}$Ra profile and (b) linear ^{228}Ra distribution on the Livingston Island transect. The solid symbols represent samples included in the calculation of the trendlines. Open symbols represent offshore samples that were excluded from the trend calculation because these may be influenced by alongshore currents that bring radium-free water from upstream locations.

which we did not measure and therefore cannot account for in calculating excess [224]Ra, may be responsible for false apparent excess [224]Ra. Due to this disparity we did not use the [224]Ra and [228]Ra activities from >250 km on the EI transect for our lateral mixing calculations. These data are indicated with open circles in Figure 5.

[20] In a system controlled by eddy diffusion, we can use the distribution of [224]Ra to calculate a horizontal eddy diffusion coefficient (K_h) [Moore, 2000a]. The distribution of this isotope with distance from the radium source will depend on two processes, radioactive decay and mixing. If advection played an important role in radium distribution and was significant in the direction toward the shelf on the transect, then the ln[224]Ra and [228]Ra profiles would take a concave shape; if advection was strong in offshore direction than the profiles would be convex. Strong alongshore advection within jets or shelf streamers may disrupt the linearity of ln[224]Ra and [228]Ra profiles, as was observed with the offshore ends of both transects (LI > 30 km, EI > 250 km) (Figures 5 and 6). As a result, these data were not included in our calculations. We did not observe any influence of advection (concave or convex shape, break in slope) on the rest of the transects (solid circles in Figures 5 and 6), therefore we assume that the system is controlled by eddy diffusion.

[21] In coastal areas, which are only the innermost stations on the LI transect, tides may also influence the radium distribution. At flood tide, high-tracer coastal waters are diluted by offshore low-radium water leading to lower tracer concentrations than at ebb tide. Due to our limited sampling schedule we could not optimize the sampling to cover low-tide and high-tide events evenly. Instead, we assume that our samples represent a midtide scenario resulting in average mixing rates.

[22] Any additional radium input such as from sediment resuspension above the shelf or from islands along the transect would disrupt the radium distribution. Since Elephant Island is the source of radium and possibly supplies new radium to the surface waters, as a precaution, on the EI transect we do not use any data that were collected above the shelf and we calculate horizontal mixing rates starting at the shelf edge (~100 km on the EI transect) downstream of which we assume no new radium inputs by vertical mixing into the surface water. We are confident in this assumption because the water depth at these stations far exceeds the depth of the mixed layer (as indicated in Table 1), which is well isolated from the sediments.

[23] Therefore at EI we derived a gradient of ln [224]Ra from the ~100 to 250 km part of the transect only (solid circles in Figure 5) in order to avoid the region influenced by radium inputs from the shelf (0–100 km) and exclude data >250 km that were influenced either by advection or supported [228]Th as discussed earlier. If the above stated assumptions hold then the ln[224]Ra slope will depend only on the decay constant λ_{224} and eddy diffusion coefficient K_h [Moore, 2000a]:

$$slope = \sqrt{\frac{\lambda_{224}}{K_h}}. \tag{1}$$

The considered part of the EI transect had a slope of -5.9×10^{-6} m^{-1} resulting in an eddy diffusion coefficient K_h of 6.3×10^4 m^2 s^{-1}. Next, we used this eddy diffusion coefficient and the concentration gradient of [228]Ra along the same transect (solid circles in Figure 5) to estimate the flux of [228]Ra from the shelf. Ra-228 in this case represents a conservative tracer as due to its long half-life it does not decay on the time scale of coastal transport processes (T$_{1/2}$ = 5.7 years). The linear [228]Ra gradient on the ~100 to 250 km part of the transect is -2.9×10^{-5} dpm m^{-3} m^{-1}. On average the surface mixed layer was 50 m, and assuming a 150 km wide shelf, the offshore [228]Ra flux was 1.2×10^{12} dpm d^{-1}. This flux is significant and exceeds estimates from other coastal regions such as 1.1×10^{11} dpm d^{-1} observed on a 240 km stretch of Brazilian coastline in the Southwest Atlantic [Windom et al., 2006] and 3.5×10^{11} dpm d^{-1} observed from a 320 km coastline in the South Atlantic Bight, USA [Moore, 2000a].

[24] The gradient of ln [224]Ra on the <30 km section of the LI transect had a slope of -6.1×10^{-5} m^{-1} (Figure 6) from which we calculated an eddy diffusion coefficient of 596 m^2 s^{-1} The linear [228]Ra gradient on the same section was -6.2×10^{-4} dpm m^{-3} m^{-1}. The [228]Ra flux from the 50 km long shoreline facing the shelf was 8.0×10^{10} dpm d^{-1}.

[25] The major difference in lateral mixing estimates on the two transects (Table 2) is due to different water circulation patterns and different mixing distance scales [Okubo, 1971]. Shelf water is entrained and mixed offshore more intensively from the EI area than from LI where surface currents offshore run westward in parallel to the islands allowing little mixing in the offshore direction [Zhou et al., 2006], hence the break in the Ra profile on the LI transect at ~30 km. These alongshore currents are steered northward by the SFZ before they reach the EI area [Zhou et al., 2006]. Differences in the mixing patterns for the two transects were also confirmed by the radium ages calculated in section 4.2.

4.2. Rapid Transport Processes Derived From Apparent Radium Water Ages

[26] Another way to express effective lateral mixing rates is to derive the time (t) over which shelf transport processes occur. We can derive this time as an apparent radium age of the offshore water masses in comparison to their age at the shelf break [Moore, 2000b]:

$$t = \ln \frac{^{224}Ra_i/^{228}Ra_i}{^{224}Ra_o/^{228}Ra_o} * \frac{1}{\lambda_{224}} \tag{2}$$

These ages are based on the faster decay of the short-lived [224]Ra (λ_{224} is the decay constant of [224]Ra in d^{-1}) in comparison to [228]Ra in an offshore water mass (Ra$_o$) assuming a known sediment end-member (Ra$_i$) and that both isotopes are subjected to the same dilution by mixing. As a zero age end-member, we use an average of the [224]Ra/[228]Ra ratio measured in the coastal zone of SSI (Table 1, sample ID 1−4, 83 and 108). We assume that all water masses have the same end-member ratio which would

Table 2. Measured and Derived Chemical and Physical Parameters on the Elephant Island and Livingston Island Transects During the January–February 2006 Study Period[a]

	EI Transect	LI Transect	Units
Transect length	300	60	km
The ln ^{224}Ra gradient	5.9×10^{-6}	6.1×10^{-5}	m^{-1}
^{228}Ra gradient	2.9×10^{-5}	6.2×10^{-4}	dpm m^{-3} m^{-1}
Horizontal eddy diffusion coefficient	6.3×10^{4}	590	m^{2} s^{-1}
The ^{228}Ra flux	1.2×10^{12}	8×10^{10}	dpm d^{-1}
DFe flux	1.1×10^{5}	1.6×10^{4}	mol d^{-1}
TalFe flux	1.1×10^{6}	8.3×10^{5}	mol d^{-1}
DFe/^{228}Ra shelf	9.5×10^{-8}	2.0×10^{-7}	mol dpm^{-1}
DFe/^{228}Ra offshore	6.2×10^{-8}	9.9×10^{-8}	mol dpm^{-1}
TalFe/^{228}Ra shelf	8.9×10^{-7}	1.0×10^{-5}	mol dpm^{-1}
TalFe/^{228}Ra offshore	2.6×10^{-7}	8.5×10^{-7}	mol dpm^{-1}
DFe residence time	4	6	d

[a]EI, Elephant Island; LI, Livingston Island.

be true if the geological material of all sediments and coastlines was similar, releasing ^{224}Ra and ^{228}Ra in the same ratio. Samples most affected by this assumption are above the shelf where the different water masses and end-members from BS, Weddell Sea and SSI mix. However, because we care mainly about the relative age difference between the samples on the shelf edge and 150 km offshore, it is a safe assumption as the choice of the end-member ratio does not change the relative difference in ages at all. On the EI transect the apparent ages increase from an average of 4.5 ± 1.5 days over the shelf to 7 ± 1 at 150 km offshore from the shelf edge, and on the LI transect from 0 nearshore to 4.5 ± 1.3 days 30 km offshore (Figure 6). The EI apparent ages are rather scattered, which results in an average age that has a relatively large standard deviation. This is a result of natural variability in water mass age due to mixing of various water masses originating in the Weddell Sea, BS and SSI along a relatively large 150 km long transect and should not be confused with measurement uncertainty. The four lowest apparent ages in Figure 7 are from the vicinity of EI, the coastal zone of which is also a source of new radium. It seems that all other samples on the transect have not been in contact with sediments for several days. Samples 150 km offshore are about 2–3 days older than

at the shelf edge. Samples beyond 150 km (≥250 km on the EI transect) are influenced by either rapid offshore transport (shelf streamers or eddies) or ^{224}Ra supported by ^{228}Th (dissolved or particulate) resulting in high ^{224}Ra/^{228}Ra ratios and zero apparent age.

[27] The large spread in ages on the beginning of the LI transect is likely due to the nonlinear nature of the shoreline and because we could not collect all samples at the same tidal stage. Ages are as high as 4–6 days at 25 km resulting in a much longer water residence time than we found on the EI transect for the same distance (Table 2).

4.3. Shelf-Derived Lateral Iron Fluxes

[28] Since iron and radium in the surface water have sources at the shelf, we can make a simplifying assumption that they have similar source functions (inputs from sediments and vertical mixing from deeper water) and convert the ^{228}Ra flux to iron flux using the concentration ratios measured above the shelf (EI) and in the coastal waters (LI). For the EI transect, the DFe to ^{228}Ra ratio on the shelf was 9.5×10^{-8} mol dpm^{-1}. Assuming the calculated ^{228}Ra flux from the shelf edge offshore this translates to an apparent dissolved iron flux of 1.14×10^{5} mol d^{-1}. The TalFe to radium ratio is 8.9×10^{-7} mol dpm^{-1} which corresponds to an apparent offshore total iron flux of 1.1×10^{6} mol d^{-1}. On the LI transect we estimate a DFe flux of 1.6×10^{4} mol d^{-1} and TalFe flux of 8.3×10^{5} mol d^{-1}. This is the amount of iron that shelf waters supply to the offshore regions. However, not all of the iron is effectively transported offshore due to scavenging or incorporation into biomass and subsequent removal from the mixed layer on sinking particles during transport. Loss of particulate Fe via settling will be due to abiotic processes (colloidal hydrolysis and subsequent scavenging by coagulation and adsorption onto sinking inorganic particles), losses of biologically incorporated Fe through sinking cell aggregates and faecal pellets and biologically mediated repackaging of small Fe particles into large sinking aggregates. The rate of iron removal from the surface layer will also vary between summer and winter seasons when there is a significant difference in primary production due to low temperatures and light limitation. Assuming that the iron source is constant year-round, from the EI region we derive an iron flux of 4.2×10^{7} mol DFe
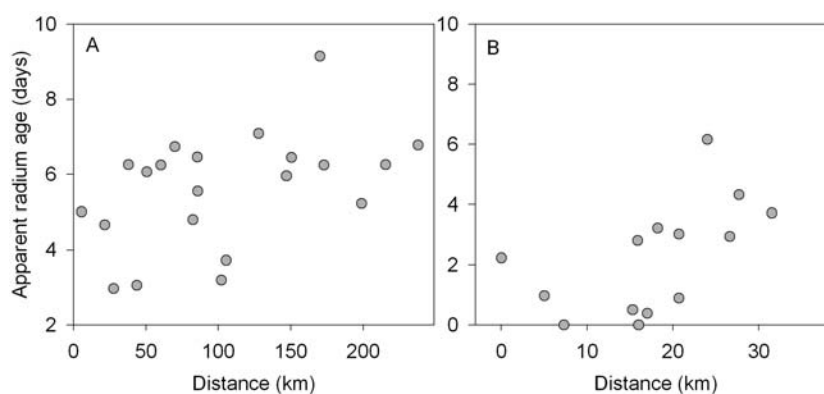

Figure 7. Apparent radium ages derived from ^{224}Ra/^{228}Ra activity ratios on the (a) EI and (b) LI transects.

yr^{-1} and 3.9×10^8 mol TalFe yr^{-1}. In the winter season this iron is transported in the mixed layer downstream of the shelf region without significant biological uptake resulting in a substantial iron inventory build up in offshore waters that may be available for uptake once light and temperature conditions are ideal in the growing season. Our study period only covered a part of the summer growing season and we observed large differences in iron inventory between the shelf and water downstream of the shelf. This iron gradient exists due to iron removal via various abiotic and biological processes mentioned above and dilution by mixing with low-iron ACC water. After corrections for dilution, net iron removal rates from the mixed layer during our study period can be estimated using Fe/Ra ratios and the derived apparent radium ages.

4.4. Summertime Iron Removal Rates From the Mixed Layer

[29] In a simplified case the loss of dissolved iron (dFe/dt) can be modeled as a first-order scavenging process limited by the dissolved free Fe concentration Fe$_i$ [*Parekh et al.*, 2004]. The rate constant $-k_{sc}$ for the dissolved iron pool represents removal by scavenging:

$$\frac{dFe}{dt} = k_{sc} * [Fe_i] \qquad (3)$$

The same equation in the integrated form yields

$$[Fe_o] = [Fe_i] \times e^{-k_{sc}t} \qquad (4)$$

To derive offshore iron concentrations [Fe$_o$], we include in equation (3) losses by horizontal mixing, which is represented by the term f_i, a fraction of the initial shelf-derived components still remaining in the water:

$$[Fe_o] = [Fe_i] \times f_i * e^{-k_{sc}t} \qquad (5)$$

The Fe data set that corresponds to our Ra stations is limited in its spatial extent; therefore we created a composite offshore Fe transect from stations located in the inner shelf and midshelf waters at LI and EI, and 150 km offshore of EI (Figure 2c). With these individual measurements we can estimate removal rates by normalizing iron to radium, which is conservative and is only subject to dilution by mixing. Assuming the same dilution of all components, we can eliminate the dilution factor f_i, by normalizing DFe to the conservative tracer ^{228}Ra:

$$\frac{[Fe_o]}{[^{228}Ra_o]} = \frac{f_i * [Fe_i] * e^{-k_{sc}t}}{f_i * [^{228}Ra_i]} \qquad (6)$$

Equation (5) then simplifies to

$$\frac{[Fe_o]}{[^{228}Ra_o]} = \frac{[Fe_i] * e^{-k_{sc}t}}{[^{228}Ra_i]}. \qquad (7)$$

The removal rate constant k_{sc} is calculated as

$$k_{sc} = \frac{\ln\left([Fe_i] \middle/ [^{228}Ra_i]\right) - \ln\left([Fe_o] \middle/ [^{228}Ra_o]\right)}{t}. \qquad (8)$$

Where t is the time scale over which these processes happen and is equal to the apparent radium age derived for these water masses. On the EI transect the offshore DFe to radium ratios were 2 to 4 times smaller then ratios on the shelf, 6×10^{-8} mol dpm^{-1}. The derived removal rate for Fe from the dissolved pool was (0.24 ± 0.10) d^{-1} and the residence time was 4 ± 1 days. On the LI transect, the offshore DFe to radium ratio was 9.9×10^{-8} mol dpm^{-1}, the removal rate was (0.16 ± 0.05) d^{-1} and the residence time was 6 ± 1 days. These estimates are conservative, representing the upper limit of residence times because we do not know the slope of the iron decrease on the transect. For TalFe the simple model of first-order removal is a crude over-simplification since the removal of particulate iron depends on incorporation into sinking aggregates. Nevertheless, the Ra/TalFe ratio decreases by as much as 4 times between the shelf and offshore region (within 4–6 days) suggesting intense iron removal from the mixed layer ((0.66 ± 0.30) d^{-1} and 1.5 ± 0.4 days for EI and (0.58 ± 0.18) d^{-1} and 1.7 ± 0.4 days for LI). A much better estimate of vertical loss of particulate Fe can be obtained by calculating a ^{234}Th based vertical particle flux.

[30] *Parekh et al.* [2004] suggested that Fe is scavenged on particles similarly to Th and that it can be used to estimate the removal of particulate Fe. We found that Th removal rates calculated based on the methods of *Coale and Bruland* [1985] were in general smaller than Fe removal (perhaps since Th is scavenged but not biologically utilized). On the EI transect the dissolved Th residence times were 150 days on the shelf and 70 days offshore in the ACC. Particulates in a size range of 1 μm < $\times$ < 54 μm had a uniform residence time of 23 days along the whole transect. Larger particles (>54 μm) had a residence time of 0.1 day above the shelf and 6 days offshore. Since we determined that lateral mixing perpendicular to the shore is favorable for offshore transport only in the EI region and not LI, we will focus on this transect. We calculated particulate Fe/Th ratios but these estimates are only approximate as we had to compare particulates from different size fractions (particulate Th > 1 μm and particulate Fe > 0.2 μm calculated as TalFe – DFe) collected at the same water depth. Also, these particulates were not collected on the same filter but on two consecutive casts with a large volume pump and GO_FLO bottles, respectively. For the EI transect the particulate Fe was 0.3 and 1.9 nM offshore and above the shelf, resulting in Fe/^{234}Th ratios of 55–70 nmol dpm^{-1} on the shelf south of EI and 0.5–2 nmol dpm^{-1} offshore. These values fit in the range of 1 to 100 nmol dpm^{-1} which encompasses estimates for particle sizes >1 μm observed in the Labrador Sea with particulate Fe of ~2.5 nM [*Weinstein and Moran*, 2005]. Based on these Fe/Th ratios and ^{234}Th/^{238}U disequilibrium (1-D steady state ^{234}Th model; Charette et al., manuscript in preparation, 2009) the net vertical Fe transport from the 50 m surface layer on the shelf

south of EI is 30 μmol Fe m^{-2} d^{-1}. We do not have export estimates in the region between the island and the shelf edge. The vertical Fe flux at sites offshore of the shelf edge is 1.5 μmol Fe m^{-2} d^{-1}. This estimate is 1−2 orders of magnitude higher than those observed by *Frew et al.* [2006] in subantarctic waters southeast of New Zealand, but comparable to *Martin et al.*'s [1990] estimate of 2 μmol Fe m^{-2} d^{-1} near the Antarctic Peninsula. Our fluxes translate to 6.1 × 10^5 mol Fe d^{-1} net vertical iron loss south of EI (2.25 × 10^{10} m^2) and 2.9 × 10^4 mol d^{-1} in the offshore region (2.25 × 10^{10} m^2) of the transect. The vertical total iron flux from the mixed layer offshore is therefore only about 25% of the dissolved horizontal iron supply of 1.14 × 10^5 mol d^{-1}. It seems that biological uptake and scavenging in the mixed layer offshore accounts for about 25% of the dissolved Fe loss which is consistent with the findings of *Frew et al.* [2006].

[31] We can estimate whether the calculated horizontal iron flux after accounting for the removal rates is sufficient to support chlorophyll *a* concentrations that were observed during our cruise in the offshore region (Figure 1). The removal processes already included biologically removed iron and particulate iron that was not initially bioavailable, hence our estimate of bioavailable dissolved iron will be conservative. A bulk estimate of new biological production supported by the amount of bioavailable iron mixed from the shelf can be made using an estimated Fe/C uptake ratio. This ratio in organisms varies among others based on macronutrient availability, light availability, differing species, Fe requirement for growth, and iron availability [*Sunda and Huntsman*, 1995; *de Baar et al.*, 1995; *Boyd et al.*, 2007; *Blain et al.*, 2007; *Frew et al.*, 2006]. Recognizing the variability of this uptake ratio on iron availability and location and depth in the water column, as an approximation we can use an average cellular Fe/C ratio of 17−25 μmol mol^{-1} determined during our cruise (Ardelan et al., manuscript in preparation, 2009). If we assume that all dissolved iron transported from the shelf is bioavailable, then the flux of 1.14 × 10^5 mol DFe d^{-1} would support a new offshore production of 4.6 × 10^9 to 6.7 × 10^9 mol C d^{-1}, equivalent to 5.5 × 10^{10} to 8.0 × 10^{10} g C d^{-1}. The measured chlorophyll *a* values (Figure 1) [*Hewes et al.*, 2006] for the offshore region were 0.5−2 mg chl *a* m^{-3},with an average of 1.5 mg chl *a* m^{-3} or 1.7 × 10^9 g for the considered area defined as the offshore 150 km part of our 150 km wide transect. In the same study region in January 1981 and 1983, for a range of 0.5−2 mg chl *a* m^{-3}, *Hewes et al.* [1990] derived C/chl *a* ratios of 116 g g^{-1} for concentrations of 0.5−1 mg chl *a* m^{-3} and 48 g g^{-1} for >2 mg chl *a* m^{-3}. In terms of carbon the measured chl *a* value of 1.7 × 10^9 g is then equivalent to 8.1 × 10^{10} to 1.9 × 10^{11} g C. This is the same range which the lateral DFe supply can sustain (5.5 × 10^{10} to 8.0 × 10^{10} g C d^{-1}). We can also compare Fe flux to Fe demand: The offshore bloom in the 150 × 150 km study area has a carbon stock of 8.1 × 10^{10} to 1.9 × 10^{11} g C, which assuming Fe/C ratios of 17−25 μmol mol^{-1} has an iron demand of 1.1 to 4 × 10^5 mol Fe. Even if we accept that after vertical removal processes only 75% of the DFe is available (which is an underestimate as some of the vertically removed iron comes from the

particulate iron pool and not the DFe inventory), then the lateral daily flux reduces to 8.5 × 10^4 mol DFe d^{-1}. With the earlier derived DFe residence time of 4 days, this input rate results in a dissolved iron inventory of 3.4 × 10^5 mol Fe (inventory = residence time × flux). This inventory is equal to the higher end of the Fe demand estimate. Considering a biological turnover time of several days and recycling within the water column [*Blain et al.*, 2007] the daily lateral iron supply should be sufficient to sustain the offshore blooms.

[32] These estimates imply that even after accounting for vertical iron losses horizontal shelf inputs alone can fully support the chl *a* concentrations in the offshore blooms (no other sources such as deepwater Fe, atmospheric deposition or other external sources are needed to balance the required iron demand). To put the lateral DFe flux in perspective we estimated the vertical upward DFe flux which represents another iron source in the offshore region. We calculated this flux using vertical eddy diffusion coefficients from the literature (1.1 × 10^{-4} to 1 × 10^{-3} m^{2}s^{-1}) [*Charette et al.*, 2007] and vertical iron profiles determined at four different stations (sample ID 25, 32, 51, 60). The vertical iron concentration slopes were ∼2.2 above the shelf and 4.8 nmol m^{-4} offshore (Ardelan et al., manuscript in preparation, 2009). Using these slopes and vertical eddy diffusion coefficients from the literature, in the offshore bloom area the vertical upward DFe fluxes were 27 to 135 nmol DFe m^{-2} d^{-1}. These represent only 7% of the lateral fluxes of 1.8 μmol Fe m^{-2} d^{-1} derived for the whole bloom area considering regions beyond our EI transect (see section 4.5). These results support the concept that relatively weak vertical particle export on the shelf and consequent weaker scavenging loss allows for transport of dissolved Fe far from source regions.

4.5. Comparison to Iron Fluxes in Other Shelf Regions in the Southern Ocean

[33] Up to this point in our calculations we assumed that lateral mixing supports iron to a limited 150 × 150 km offshore area covered by the offshore part of the EI transect. However, incomplete Fe removal from the mixed layer allows iron to be transported farther offshore. The lateral Fe supply of 1.14 × 10^5 mol DFe d^{-1} derived in this study scaled up for the whole bloom area of 250 × 250 km north of Elephant Island (Figure 1) would be 1.8 μmol Fe m^{-2} d^{-1}, which assuming Fe/C ratios of 17−25 μmol mol^{-1} would support a production of 0.07 to 0.11 mol C m^{-2} d^{-1}. Similarly to other studies we found that these lateral fluxes were significantly higher than vertical upward DFe fluxes (27 to 135 nmol DFe m^{-2} d^{-1}). Other studies showed lateral iron fluxes of similar magnitude and significance.

[34] *Charette et al.* [2007] found that lateral inputs of Fe from the Crozet Plateau dominated over vertical sources. These authors also used radium isotopes as tracers of lateral and vertical mixing. Radium-223 and ^{224}Ra trends yielded horizontal eddy diffusivities of 39 and 6.6 m^2 s^{-1} on a 15 km long transect and vertical mixing rates (derived from ^{228}Ra) of 11−100 cm^2 s^{-1} in the upper 300 m. The corresponding vertical Fe flux was 5.6 to 31 nmol Fe m^{-2} d^{-1} as opposed to lateral fluxes from the plateau

sediments of $64-390$ nmol Fe m^{-2} d^{-1}. These fluxes were fueling a carbon uptake of 15 to 24 mmol C m^{-2} d^{-1} [*Lucas et al.*, 2007]. Although the scale of this transect is an order of magnitude lower resulting in lower Fe fluxes, the conclusion of this study is the same as ours, that lateral Fe fluxes from the shelf are significant.

[35] In the naturally fertilized Kerguelen Plateau, *Blain et al.* [2007] found vertical Fe fluxes of 4 nmol Fe m^{-2} d^{-1} in the nonfertilized region off the shelf and 31 nmol Fe m^{-2} d^{-1} in the naturally iron-fertilized region, which is close to our lower-limit vertical flux estimate and 2 orders of magnitude lower than our horizontal fluxes. The authors found that even this elevated vertical DFe supply in the fertilized region above the plateau did not meet the net DFe demand of phytoplankton (208 nmol m^{-2} d^{-1}). They suggested that dissolution of lithogenic Fe may be an additional important DFe source. At the same site, based on ^{228}Ra measurements and physical oceanographic data, *van Beek et al.* [2008] concluded that lateral fluxes probably by advection of high-Fe waters off Heard Island contribute significant amounts of iron into the Kerguelen Plateau and may balance the required iron demand. *Zhang et al.* [2008] reached the same conclusion using dissolved rare earth element distributions and calculated that the Heard Island region provides 5×10^6 mol of dissolved iron d^{-1}, some of which is potentially transported northward to the Kerguelen Plateau region. *Zhang et al.*'s [2008] estimate of iron flux is higher than ours but shows that fluxes of such magnitude are not uncommon from extensive shelf regions such as the Kerguelen Plateau or the shelf of the SSI.

[36] These studies show that the island mass effect and lateral iron fluxes from extensive shelf regions are indeed important and provide ample iron supply to account for the biological DFe demand in the Southern Ocean. In our case, if we assumed a constant DFe supply year-round (4.2×10^7 mol DFe yr^{-1}), then in the growing season the net DFe supply without considering the reuse of recycled iron, would produce plankton equivalent to 1.7 to 2.4×10^{12} mol C yr^{-1}.

5. Conclusions

[37] Based on radium and iron measured on transects leading from the shelf of the SSI to offshore regions of the southern Drake Passage we demonstrated that shelf water entrainment into HNLC ACC waters can be an effective transport mechanism for biolimiting micronutrients such as iron. We investigated two different transects, one of which leads through the shelf around EI, a region that proved to be a significant source of shelf-derived components for offshore waters. The presence of excess ^{224}Ra and ^{228}Ra in surface waters several hundreds of km from the shelf edge suggests rapid horizontal mixing of entrained shelf water offshore. Elevated iron from the shelf is quickly transported offshore where it can fuel plankton blooms. On the other transect on the shelf near LI, the water residence time was ten times longer than near EI and alongshore currents prevailed over net offshore (>100 km) transport. This region did not supply significant amounts of Ra or Fe into the offshore waters.

[38] To estimate how much of this shelf-derived iron is truly available in the offshore waters we estimated the removal rates of dissolved and particulate iron from the mixed layer on the EI transect. Based on ^{234}Th-derived particle export, most of the iron is removed from the mixed layer by vertical transport after biological uptake and scavenging with a bulk residence time of 4 days. We determined that, despite of the vertical removal rates (25% of total flux), there was enough iron left to fuel phytoplankton blooms in the offshore region; this laterally transported dissolved iron is sufficient to sustain chlorophyll levels of $0.5-2$ mg m^{-3} observed during our study.

References

Baffi, F., and A. Cardinale (1990), Improvements in use of Chelex-100 resin for determination of copper, cadmium and iron in sea water, *Int. J. Anal. Chem.*, *41*, 15–20, doi:10.1080/03067319008030524.

Barbeau, K., et al. (2006), Phytoplankton iron stress across chlorophyll and dissolved iron gradients in the southern Drake Passage, *Eos Trans. AGU*, *87*(36), Ocean Sci. Meet. Suppl., Abstract OS33F-05.

Berelson, W., J. McManus, K. Coale, K. Johnson, T. Kilgore, D. Burdige, and C. Pilskaln (1996), Biogenic matter diagenesis on the sea floor: A comparison between two continental margin transects, *J. Mar. Res.*, *54*, 731–762, doi:10.1357/0022240963213673.

Berelson, W., J. McManus, K. Coale, K. Johnson, D. Burdige, T. Kilgore, D. Colodner, F. Chavez, R. Kudela, and J. Boucher (2003), A time-series of benthic flux measurements from Monterey Bay, CA, *Cont. Shelf Res.*, *23*, 457–481, doi:10.1016/S0278-4343(03)00009-8.

Blain, S., et al. (2001), A biogeochemical study of the island mass effect in the context of the iron hypothesis: Kerguelen Islands, Southern Ocean, *Deep Sea Res., Part I*, *48*, 163–187, doi:10.1016/S0967-0637(00)00047-9.

Blain, S., et al. (2007), Effect of natural iron fertilization on carbon sequestration in the Southern Ocean, *Nature*, *446*, 1070–1075, doi:10.1038/nature05700.

Boyd, P. W., and D. Mackie (2008), Comment on "The Southern Ocean biological response to Aeolian iron deposition", *Science*, *319*, 159, doi:10.1126/science.1149884.

Boyd, P. W., et al. (2007), Mesoscale iron enrichment experiments 1993–2005: Synthesis and future directions, *Science*, *315*, 612–617, doi:10.1126/science.1131669.

Buesseler, K. O., L. Ball, J. Andrews, C. Benitez-Nelson, R. Belastock, F. Chai, and Y. Chao (1998), Upper ocean export of particulate organic carbon in the Arabian Sea derived from Thorium-234, *Deep Sea Res., Part II*, *45*(10–11), 2461–2487.

Charette, M. A., M. E. Gonneea, P. J. Morris, P. Statham, G. Fones, H. Planquette, I. Salter, and A. N. Garabato (2007), Radium isotopes as tracers of iron sources fueling a Southern Ocean phytoplankton bloom, *Deep Sea Res., Part II*, *54*, 1989–1998, doi:10.1016/j.dsr2.2007.06.003.

Coale, K. H., and K. W. Bruland (1985), ^{234}Th:^{238}U disequilibria within the California Current, *Limnol. Oceanogr.*, *30*(l), 22–33.

Coale, K. H., et al. (1996), A massive phytoplankton bloom induced by an ecosystem-scale iron fertilization experiment in the equatorial Pacific Ocean, *Nature*, *383*, 495–501, doi:10.1038/383495a0.

de Baar, H. J. W., J. T. M. de Jong, D. C. E. Bakker, B. M. Löscher, C. Veth, U. Bathmann, and V. Smetacek (1995), Importance of iron for plankton blooms and carbon dioxide drawdown, *Nature*, *373*, 412–415, doi:10.1038/373412a0.

Elrod, V. A., W. M. Berelson, K. H. Coale, and K. S. Johnson (2004), The flux of iron from continental shelf sediments: A missing source for global budgets, *Geophys. Res. Lett.*, *31*, L12307, doi:10.1029/2004GL020216.

Frew, R. D., D. A. Hutchins, S. Nodder, S. Sanudo-Wilhelmy, A. Tovar-Sanchez, K. Leblanc, C. E. Hare, and P. W. Boyd (2006), Particulate iron dynamics during Fe cycle in subantarctic waters southeast of New Zealand, *Global Biogeochem. Cycles*, 20, GB1S93, doi:10.1029/2005GB002558.

Geibert, W. (2001), Actinium-227 as a tracer for advection and mixing in the deep sea, *Rep. Polar Mar. Res.*, 385, 112 pp.

Geibert, W., M. M. Rutgers van der Loeff, C. Hanfland, and H.-J. Dauelsberg (2002), Actinium-227 as a deep-sea tracer: Sources, distribution and applications, *Earth Planet. Sci. Lett.*, 198, 147–165, doi:10.1016/S0012-821X(02)00512-5.

Grotti, M., F. Soggia, M. Abelmoschi, P. Rivaro, E. Magi, and R. Frache (2001), Temporal distribution of trace metals in Antarctic coastal waters, *Mar. Chem.*, 76, 189–209, doi:10.1016/S0304-4203(01)00063-9.

Hanfland, C. (2002), Radium-226 and radium-228 n the Atlantic sector of the Southern Ocean, Ph.D. thesis, 137 pp., Alfred-Wegener Inst. for Polar and Mar. Res., Bremerhaven, Germany.

Hewes, C. D., E. Sakshaug, O. Holm-Hansen, and F. M. H. Reid (1990), Microbial autotrophic and heterotrophic eucaryotes in Antarctic waters: Relationships between biomass and chlorophyll, adenosine triphosphate and particulate organic carbon, *Mar. Ecol. Prog. Ser.*, 63, 27–35, doi:10.3354/meps063027.

Hewes, C. D., et al. (2006), Phytoplankton studies, in *AMLR 2005/2006 Field Season Report, Objectives, Accomplishments and Tentative Conclusions, NOAA-TM-NMFS-SWFSC-397*, edited by J. D. Lipsky, pp. 31–46, Antarct. Ecosyst. Res. Div., Southwest Fish. Sci. Cent., Natl. Mar. Fish. Serv., NOAA, U.S. Dept. of Comm., La Jolla, Calif.

Holm-Hansen, O., C. D. Hewes, V. E. Villafane, E. W. Helbling, N. Silva, and T. Amos (1997), Distribution of phytoplankton and nutrients in relation to different water masses in the area around Elephant Island, *Antarctica, Polar Biol.*, 18, 145–153, doi:10.1007/s003000050169.

Hopkinson, B. M., B. G. Mitchell, R. A. Reynolds, H. Wang, K. E. Selph, C. I. Measures, C. D. Hewes, O. Holm-Hansen, and K. A. Barbeau (2007), Iron limitation across chlorophyll gradients in the southern Drake Passage: Phytoplankton responses to iron addition and photosynthetic indicators of iron stress, *Limnol. Oceanogr.*, 52(6), 2540–2554.

Jickells, T. D., et al. (2005), Global iron connections between desert dust, ocean biogeochemistry, and climate, *Science*, 308, 67–71, doi:10.1126/science.1105959.

Johnson, K. S., R. M. Gordon, and K. H. Coale (1997), What controls dissolved iron in the world ocean?, *Mar. Chem.*, 57, 137–161, doi:10.1016/S0304-4203(97)00043-1.

Kadko, D., and R. Muench (2005), Evaluation of shelf-basin interaction in the western Arctic by use of short-lived radium isotopes: The importance of mesoscale processes, *Deep Sea Res., Part II*, 52, 3227–3244, doi:10.1016/j.dsr2.2005.10.008.

Kaufman, A., R. M. Trier, W. S. Broecker, and W. H. Feely (1973), Distribution of ^{228}Ra in the world ocean, *J. Geophys. Res.*, 78, 8827–8848, doi:10.1029/JC078i036p08827.

Klinkhammer, G. P., C. S. Chin, R. A. Keller, A. H. Dählmann, A. Sahling, G. Sarthou, S. Petersen, F. Smith, and C. Wilson (2001), Discovery of new hydrothermal vent sites in Bransfield Strait, Antarctica, *Earth Planet. Sci. Lett.*, 193, 395–407, doi:10.1016/S0012-821X(01)00536-2.

Li, Y.-H., G. Mathieu, P. Biscaye, and H. J. Simpson (1977), The flux of ^{226}Ra from estuarine and continental shelf sediments, *Earth Planet. Sci. Lett.*, 37, 237–241, doi:10.1016/0012-821X(77)90168-6.

Löscher, B. M., H. J. W. de Baar, J. T. M. de Jong, C. Veth, and F. Dehairs (1997), The distribution of Fe in the Antarctic Circumpolar Current, *Deep Sea Res., Part II*, 44, 143–187, doi:10.1016/S0967-0645(96)00101-4.

Lucas, M., S. Seeyave, R. Sanders, C. M. Moore, R. Williamson, and M. Stinchcombe (2007), Nitrogen uptake responses to a naturally Fe-fertilised phytoplankton bloom during the 2004/2005 CROZEX study, *Deep Sea Res., Part II*, 54, 2138–2173, doi:10.1016/j.dsr2.2007.06.017.

Luther, W. L., and J. Wu (1997), What controls dissolved iron concentrations in the world ocean?: A comment, *Mar. Chem.*, 57(3–4), 173–179, doi:10.1016/S0304-4203(97)00046-7.

Martin, J. H., and S. E. Fitzwater (1988), Iron deficiency limits phytoplankton growth in the north-east subarctic Pacific, *Nature*, 331, 341–343, doi:10.1038/331341a0.

Martin, J. H., S. Fitzwater, and R. M. Gordon (1990), Iron deficiency limits phytoplankton growth in Antarctic waters, *Global Biogeochem. Cycles*, 4(1), 5–12, doi:10.1029/GB004i001p00005.

Martin, J. H., R. M. Gordon, and S. E. Fitzwater (1991), What controls phytoplankton production in nutrient-rich areas of the open sea?, *Limnol. Oceanogr.*, 36(8), 1793–1802.

Mitchell, B. G., and O. Holm-Hansen (1991), Bio-optical properties of Antarctic Peninsula waters: Differentiation from temperate ocean models, *Deep Sea Res.*, 38, 1009–1028, doi:10.1016/0198-0149(91)90094-V.

Moore, W. S. (1996), Large groundwater inputs to coastal waters revealed by ^{226}Ra enrichments, *Nature*, 380, 612–614, doi:10.1038/380612a0.

Moore, W. S. (2000a), Determining coastal mixing rates using radium isotopes, *Cont. Shelf Res.*, 20, 1993–2007, doi:10.1016/S0278-4343(00)00054-6.

Moore, W. S. (2000b), Ages of continental shelf waters determined from ^{223}Ra and ^{224}Ra, *J. Geophys. Res.*, 105(C9), 22,117–22,122, doi:10.1029/1999JC000289.

Moore, W. S., and R. Arnold (1996), Measurement of ^{223}Ra and ^{224}Ra in coastal waters using delayed coincidence counter, *J. Geophys. Res.*, 101(C1), 1321–1329, doi:10.1029/95JC03139.

Okubo, A. (1971), Oceanic diffusion diagrams, *Deep Sea Res.*, 18, 789–802.

Orsi, A. H., T. Whitworth, and W. D. Nowlin (1995), On the meridional extent and fronts of the Antarctic circumpolar current, *Deep Sea Res., Part I*, 42, 641–673, doi:10.1016/0967-0637(95)00021-W.

Öztürk, M. (1995), Trends of trace metals (Mn, Fe, Co, Cu, Zn, Cd and Pb) distributions at the oxic-anoxic interface and in sulfidic water of Drammensfjord, *Mar. Chem.*, 48, 329–342, doi:10.1016/0304-4203(95)92785-Q.

Öztürk, M., E. Steinnes, and E. Sakshaug (2002), Iron speciation in the Trondheim Fjord from the perspective of iron limitation for phytoplankton, *Estuar. Coastal Sci.*, 55, 197–212, doi:10.1006/ecss.2001.0897.

Parekh, P., M. J. Follows, and E. Boyle (2004), Modeling the global ocean iron cycle, *Global Biogeochem. Cycles*, 18, GB1002, doi:10.1029/2003GB002061.

Planquette, H., et al. (2007), Dissolved iron in the vicinity of the Crozet Islands, Southern Ocean, *Deep Sea Res., Part II*, 54, 1999–2019, doi:10.1016/j.dsr2.2007.06.019.

Rasmussen, L. (2003), Radium isotopes as tracers of coastal circulation pathways in the mid-Atlantic Bight, Masters thesis, Ken Buesseler, Advisor, WHOI-MIT Joint program, Cambridge, Mass.

Schmidt, S., and J.-L. Reyss (1996), Radium as internal tracer of Mediterranean outflow, *J. Geophys. Res.*, 101(C2), 3589–3596, doi:10.1029/95JC03308.

Smith, K. L., B. H. Robinson, J. J. Helly, R. S. Kaufman, H. A. Ruhl, T. J. Shaw, B. S. Twining, and M. Vernet (2007), Free-drifting icebergs: Hot spots of chemical and biological enrichment in the Weddell Sea, *Science*, 317, 478–482, doi:10.1126/science.1142834.

Sunda, W. G., and S. A. Huntsman (1995), Iron uptake and growth limitation in oceanic and coastal phytoplankton, *Mar. Chem.*, 50, 189–206, doi:10.1016/0304-4203(95)00035-P.

van Beek, P. V., M. Bourquin, J.-L. Reyss, M. Souhaut, M. A. Charette, and C. Jeandel (2008), Radium isotopes to investigate the water mass pathways on the Kerguelen Plateau (Southern Ocean), *Deep Sea Res., Part II*, 55, 622–637, doi:10.1016/j.dsr2.2007.12.025.

Wagener, T., C. Guieu, R. Losno, S. Bonnet, and N. Mahowald (2008), Revisiting atmospheric dust export to the Southern Hemisphere ocean: Biogeochemical implications, *Global Biogeochem. Cycles*, 22, GB2006, doi:10.1029/2007GB002984.

Weinstein, S., and S. B. Moran (2005), Vertical Flux of particulate Al, Fe, Pb, and Ba from the upper ocean estimated from ^{234}Th/^{238}U disequilibria, *Deep Sea Res., Part I*, 52, 1477–1488, doi:10.1016/j.dsr.2005.03.008.

Windom, H. L., W. S. Moore, L. F. Niencheski, and R. A. Jahnke (2006), Submarine groundwater discharge: A large, previously unrecognized source of dissolved iron to the South Atlantic Ocean, *Mar. Chem.*, 102, 252–266, doi:10.1016/j.marchem.2006.06.016.

Zhang, L., Z. Liu, J. Zhang, G. H. Hong, Y. Park, and H. F. Zhang (2007), Reevaluation of mixing among multiple water masses in the shelf: An example from the East China Sea, *Cont. Shelf Res.*, 27(15), 1969–1979, doi:10.1016/j.csr.2007.04.002.

Zhang, Y., F. Lacan, and C. Jeandel (2008), Dissolved rare earth elements tracing lithogenic inputs over the Kerguelen Plateau (Southern Ocean), *Deep Sea Res., Part II*, 55, 638–652, doi:10.1016/j.dsr2.2007.12.029.

Zhou, M., P. P. Niller, Y. Zhu, and R. D. Dorland (2006), The western boundary current in the Bransfield Strait, Antarctica, *Deep Sea Res., Part I*, 53(7), 1244–1252, doi:10.1016/j.dsr.2006.04.003.

————————————

M. V. Ardelan, Department of Chemistry, Norwegian University of Science and Technology, Trondheim NO-7491, Norway.

M. A. Charette and P. B. Henderson, Department of Marine Chemistry and Geochemistry, Woods Hole Oceanographic Institution, Woods Hole, MA 02543, USA.

H. Dulaiova, Department of Geology and Geophysics, University of Hawaii, Honolulu, HI 96822, USA. (hdulaiov@hawaii.edu)